

APPROACHES TO MITIGATE DISRUPTION OF TELEMETRY DURING DIRECTED ENERGY TESTING*

Michael Keidar and Madhusudhan Kundrapu
The George Washington University, Washington D.C.

Minkwan Kim and Iain D. Boyd
Department of Aerospace Engineering, University of Michigan, Ann Arbor, Michigan

Charles H. Jones and Brian Mork
Air Force Flight Test Center, Edwards Air Force Base, California

ABSTRACT

Testing of directed-energy weapon systems requires continuous radio-wave telemetry in order to characterize in situ the effect of irradiation on a target. The telemetry in these cases might be disrupted due to plasma formation causing communication blackout. In this paper several mitigation approaches, namely electrostatic and electromagnetic, are considered. The electrostatic mitigation approach takes into account that an electron depleted sheath is formed around the negatively biased electrode. This creates a 'hole' in the electron density distribution allowing radio communication through the plasma. The electromagnetic approach is based on formation of the ExB layer in the plasma, consequent plasma acceleration, and resulting decrease in the plasma density.

In order to assess these mitigation approaches, one needs to characterize the plasma which is created as a result of laser irradiation on different target materials and under various laser beam power levels. We developed a model of the plasma formation which is based on a kinetic description of the Knudsen layer and a hydrodynamic description of the collision-dominated plasma region which is coupled with analyses of the heat transfer in the target material. The overall model describes the absorption of the laser energy by the target and the resulting temperature rise in the surface. This temperature rise then induces ablation of the target material. Laser energy absorption by the plasma plume created above the surface is also considered. Analysis of the ablation rate of various targets subject to directed energy impact was performed. We considered a typical multilayer structure consisting of black paint, titanium, and aluminum layers. For instance, it was found that the aluminum layer has the highest ablation rate, while the black paint layer has the smallest rate for a given surface temperature.

*This research is supported by the Air Force Office of Scientific Research, grant number FA9550-06-1-0393 (Dr. John D. Schmisser is the manager).

INTRODUCTION

Testing and evaluation of the directed energy weapon system requires continuous radio-wave telemetry in order to characterize in situ the effects of laser irradiation on different target materials. Unfortunately, the incident radiation can cause disruption of the radio signal during the directed-energy testing. Several phenomena associated with directed-energy impact can lead to communication path losses, such as ablation, charged particle emission, charring, and chemical changes in the target materials. The incidence of a high-power laser pulse onto a material leads to local heating and consequent ablation. The ablated material continues to expand, compressing the air and forming a shock wave. Within the plasma and near the shock front, the combination of high-air temperatures and the ablated material causes complex chemical reactions leading to ionization, recombination, and excitation. In addition, chemical reactions between the ablated material and air molecules are possible at these elevated air temperatures.

There have been a number of numerical models proposed to analyze the laser-solid interaction and ablation process¹⁻¹⁵. The main advance in this study is self-consistent treatment of the ablation, heat transfer, plasma generation, and plasma-laser interactions. In particular, we developed a model of the plasma formation based on a kinetic description of the Knudsen layer and a hydrodynamic description of the collision-dominated plasma region. Our project is focused on the ablation of metals with high laser fluences varying from 1 to 100 J/cm² with beam diameter of 1 to 50 cm. Enthalpy model¹⁶⁻¹⁸ is considered for heat diffusion, as it does not require information of solid-liquid phase fronts.

Our model describes the absorption of the laser energy by the target and the resulting temperature rise in the surface. This temperature rise induces ablation of the target material. Results for an aluminum target irradiated with a KrF laser were obtained from the model. Laser energy absorption by the plasma plume created above the surface was also considered. Analysis of the ablation rate of various targets subject to directed energy impact was performed. It was found that the ablation rate depends on the surface temperature as well as plasma density in the target vicinity. We considered a typical multilayer structure consisting of carbon, titanium, and aluminum layers. It was found that the aluminum layer has the highest ablation rate, while the carbon layer has the smallest rate for a given surface temperature. In addition, electrostatic and electromagnetic mitigation techniques were developed to allow direct radio communication through the plasma layer.

MODEL DESCRIPTION: LASER-TARGET INTERACTION

In the following we briefly describe the overall model. More details about the model can be found elsewhere¹⁶. We consider the laser beam of a Gaussian profile having fluencies as the parameter. Schematically laser-target interaction is presented in figure 1.

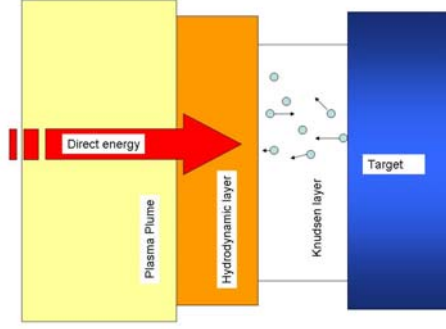


Figure 1 Schematic of Directed Energy (DE) Interactions

The surface temperature of the target material due to the laser beam was computed from the following equation¹⁶,

$$c\rho \frac{\partial T(z,t)}{\partial t} = \nabla \{K(T(z,t))\nabla T(z,t)\} + q_{laser}(z,t) \quad (1)$$

where c is the specific heat of the material, ρ is the density, K is the temperature dependent heat conductivity, and q_{laser} is the heat source due to the absorption of laser radiation. The heat source term in Eq. (1) is given by

$$q_{laser}(z,t) = \mu(z)I(z,t) \quad (2)$$

where μ is the absorption coefficient and I is the laser beam irradiance, and is given as

$$I(z,t) = AI_o(t) \exp\left[-\int_0^z \mu(z,t)dz\right] \quad (3)$$

where A is the surface absorptivity and I_o is the irradiance of the incident beam. Laser irradiances in the range of 0.1 to 30 kW/cm² were considered. The effects of convective heat exchange with the external airflow, thermal radiation from the surface, and evaporation of the metal surface will also be incorporated in order to obtain an accurate description of the thermal field in the target material; thereby, providing an accurate surface temperature for use with the kinetic model for ablation. Assuming quasi-neutrality in the plasma and local thermodynamic equilibrium (LTE), the electron temperature can be obtained from the energy balance equation written in this form¹⁶

$$\frac{3}{2}n_e V \frac{\partial T_p}{\partial z} = Q_{IB} - Q_{ei} - Q_\lambda \quad (4)$$

where T_p is the electron temperature, n_e is the electron density, Q_{ei} is the rate of energy transfer from electrons to ions, Q_λ is the rate of energy transfer due to thermal conductivity, and Q_{IB} is the power density absorbed by electrons via the inverse bremsstrahlung effect, given by

$$Q_{IB} = \alpha_{IB} I_o \exp(-\alpha_{IB} x) \quad (5)$$

where I_o is the laser power density, and α_{IB} is the inverse bremsstrahlung coefficient. This coefficient can be calculated as

$$\alpha_{IB} = 1.37 \times 10^{-35} \lambda^3 n_e^2 T_e^{-1/2} \quad (6)$$

where λ is the laser wavelength in microns and α_{IB} is in units of cm^{-1} . The electron density in the previous equations can be calculated from the Saha equation^{1,12} once the plasma density has been obtained. The plasma density at the surface can be determined if the equilibrium vapor pressure can be specified. The following relation⁵ gives the equilibrium pressure as

$$\log p = A - \frac{B}{T_0} \quad (7)$$

where A and B are parameters of a given metal and T_0 is the temperature at the surface. The equation of state $P = n_0 k T_0$ can then be used to calculate the density at the surface.

The heating of the target and subsequent ablation of material forms a plume in the vacuum above the surface that continues to develop with increasing temperature and density, causing the ionization of the vapor and the formation of a plasma. This rise in temperature and density means the collisions between particles becomes frequent enough for the assumption of local thermodynamic equilibrium to be adopted for the description of the plume expansion. This assumption implies that thermal equilibrium is established between neutrals, ions, and electrons in a sufficiently small region of the vapor and a common temperature can be used to characterize them. Furthermore, the Saha equation can then be employed to determine the fraction of electrons, ions, and neutrals in the vapor. The expansion of the vapor in the vicinity of the ablated target is modeled using the Euler equations^{12,19}. The system of equations includes the conservation of energy, momentum, and energy.

MODEL DESCRIPTION: MITIGATION APPROACHES

Electromagnetic Approach

In this section, we introduce the electromagnetic, cross electric and magnetic fields (ExB) layer to reduce the plasma number density. In this approach, we consider two different limiting cases which are the plasma-optic regime and the magneto-hydro-dynamic (MHD) regime, respectively. The plasma-optic regime has a partially magnetized plasma which means ions are unmagnetized and electrons are magnetized. In the MHD regime, both the ions and the electrons are magnetized. The regimes occur under different plasma number density conditions. The E×B drift is the main acceleration factor in the plasma-optic regime. The main issue of this regime is the maintenance of a strong electric field across the magnetic field. However, at a relatively dense plasma condition, ion acceleration is still possible but requires a stronger magnetic field. Under this case, ion-neutral coupling becomes more important than the relatively low density plasma condition. The strong ion-neutral coupling means that ions and neutrals act as one fluid. In this

case, we need to consider magnetized ions. This is called the MHD regime, which is considered at a relatively dense plasma condition. The main acceleration mechanism of the MHD regime is the JxB drift. The applied hydrodynamic model is described as follows:

$$\nabla \cdot (\mathbf{V}_i n_i) = 0 \quad (8)$$

$$m_i n_i (\mathbf{V}_i \cdot \nabla \mathbf{V}_i) = e n_i (\mathbf{E} + \mathbf{V}_i \times \mathbf{B}) - \nabla \mathbf{P}_i - m_e n_e \nu_{ie} (\mathbf{V}_i - \mathbf{V}_e) - m_i n_i \nu_{in} (\mathbf{V}_i - \mathbf{V}_n) \quad (9)$$

$$0 = -e n_e (\mathbf{E} + \mathbf{V}_e \times \mathbf{B}) - \nabla \mathbf{P}_e - m_e n_e \nu_{ei} (\mathbf{V}_e - \mathbf{V}_i) - m_e n_e \nu_{en} (\mathbf{V}_e - \mathbf{V}_n) \quad (10)$$

Equation (8) describes ion mass conservation and equations. (9) and 10) describe ion and electron momentum conservation, respectively. Equations (8) through (10) can be simplified using the following general assumptions:

- (1) The ExB layer is quasi-neutral
- (2) The neutrals are at rest
- (3) There is no ionization in the ExB layer
- (4) T_e is constant

The assumption that neutrals are at rest maximizes the effect of the ion-neutral drag term. Because the ion temperature is relatively small compared with the electron temperature, the ion pressure term of Eq. (9) is negligible. In the MHD regime, we assume that the ion and electron velocities are the same because there is no current generation due to the ExB drift.

Electrostatic Approach

As a possible method to reduce electron density in the plasma layer and, thus to, increase possibility for direct radio communication through the plasma layer, we introduce the electrostatic plasma sheath. When a negative voltage is applied to a cathode in a plasma, a plasma sheath is formed. Because electrons are depleted from the sheath, the sheath generates a region of depleted electron density area, a ‘hole.’ Since the ‘hole’ has a negligible number of electrons, it gives a possibility of communication through the plasma layer. For this case, the size of the plasma hole is important since it must contain the physical size of the transmission and/or reception antennas. Before we consider a two-dimensional sheath, we need to look at the one-dimensional case. In the one-dimensional steady state case, the sheath thickness can be estimated according to the Child-Langmuir law².

$$s = \left(\frac{4}{9} \varepsilon_0 \right)^{1/2} \left(\frac{2Z_i e}{m_i} \right)^{1/4} \frac{U^{3/4}}{(eZ_i n V)^{1/2}} \quad (11)$$

where V is the ion velocity at the sheath edge, U is the voltage across the sheath, s is the sheath thickness, ε_0 is the permittivity of vacuum, Z_i is the ion mean charge number, n is the plasma density at the sheath edge, and m_i is the ion mass. It is obvious that the steady-state sheath

thickness is determined by plasma density and ion velocity at the sheath edge for a given bias voltage.

In the two-dimensional case, we use the steady state two-dimensional fluid sheath model which is based on the time-dependent fluid sheath model. Two main assumptions are applied in the collisional sheath modeling. First, it is assumed that the sheath has a uniform background neutral density and the ions are cold. The uniform background neutral density introduces collision drag terms into the two-dimensional fluid sheath model. The ion pressure term of the ion momentum equation is negligible due to the cold ion assumption. Next, the electrons are assumed to satisfy the Boltzmann relation in the sheath model which can be coupled with Poisson's equation for the electric potential. The electron distribution in the sheath depends on the electron temperature (typically is about 1 to 1.5 eV)¹⁶ and the potential distribution in the sheath.

RESULTS

Figure 2 shows the penetration profiles of a three-layer metal configuration due to ablation for three given surface temperatures of 5,500, 6,000, and 6,500 K. The ablation rates were calculated using the kinetic model that was used in this study, and the rate of penetration was then obtained by considering the loss of material from the surface. The results of the present study can also be used to investigate the rate of penetration into materials due to ablation induced by laser irradiance.

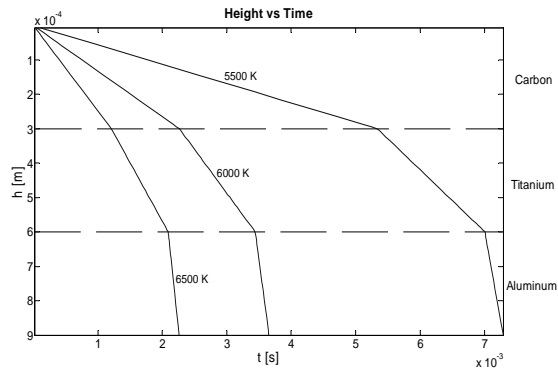


Figure 2 Penetration into Multilayered Structure

The laser pulse assumed in this study had a Gaussian profile with full width at half maximum (FWHM) of 8 nanoseconds (ns), and centered at 15 ns. Furthermore, a KrF laser was modeled, with wavelength, λ , of 248 nm. In this study, the laser fluence was chosen as the parameter, and the laser beam intensity was calculated to produce the required fluence. Fluences in the range of 3.0 to 8.0 J/cm² were considered in this paper.

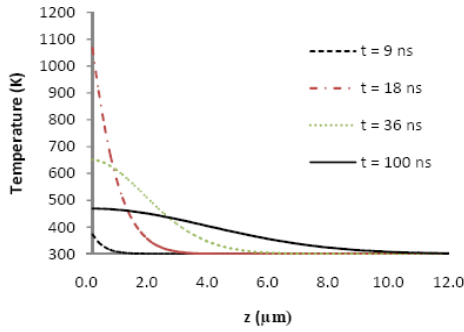


Figure 3 Temperature Distribution in the Target with Time as a Parameter

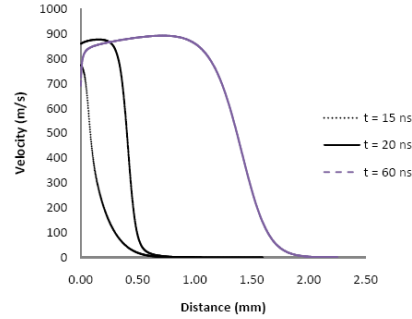


Figure 4. Velocity Distribution in the Plasma Plume with Time as a Parameter

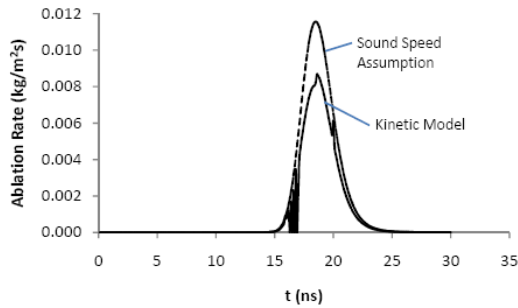


Figure 5 Ablation Rate Temporal Behavior

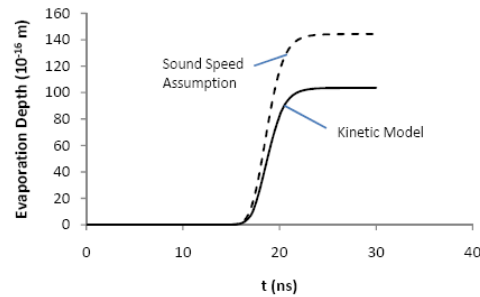


Figure 6 Evaporation Rate Temporal Behavior

Aluminum was chosen as the target because it is a material of interest and to allow for comparison of the results with other models.

Initially, the aluminum target is at room temperature of 300 K. As a result of the incident laser beam, the target will be heated. The temperature distribution in the target material is plotted at several representative times in Fig. 3. As expected, the temperature is maximum at the surface for all times. Initially the temperature near the surface rises quickly as the laser beam intensity reaches its highest value at 15 ns. The maximum temperature is achieved at the surface several nanoseconds after the peak laser intensity. After this, the surface temperature, as well as the temperature in the target, begins to drop as the amount of energy being absorbed is reduced. The temperature gradients in the target also decrease and a smoother profile is observable at longer times. It can also be observed that the heat conduction penetrates to about 10 μm into the material in 100 ns. Target material heating leads to evaporation. Evaporated material rapidly expands as shown in Fig. 4.

The heating of the aluminum target will cause the target material to start evaporating, and the ablation rate will generally increase as the surface temperature increases. The ablation rate of the aluminum during the laser irradiance is shown in Fig. 4. The results indicate that the ablation rate increases sharply as the target surface temperature rises, and begins dropping as the laser beam intensity drops and the surface temperature decreases. In fact, the vaporization of material is one of the factors causing the surface temperature to drop. In general, two approaches to calculate the ablation rate were developed. One is to assume that the plume expands to sound speed at the edge of the Knudsen layer^{4,8-12} and the other is to solve self-consistently the kinetic Knudsen

layer and plasma formation problems proposed earlier² and implemented in this paper. Figures 5 and 6 show the difference in using these approaches to calculate the ablation rate and evaporation depth. It should be pointed out that effect of the coupling is very important in evaporation depth predictions and should be taken into account.

Let us consider the plasma density distribution in the case of a two-dimensional sheath in the front of the negative electrode. Because the applied voltage (1,000 V) is large compared with the electron temperature (1 to 1.5 eV), the electrons are depleted near the negative electrode and the main question is the spatial extent of the depleted region, the ‘hole’.

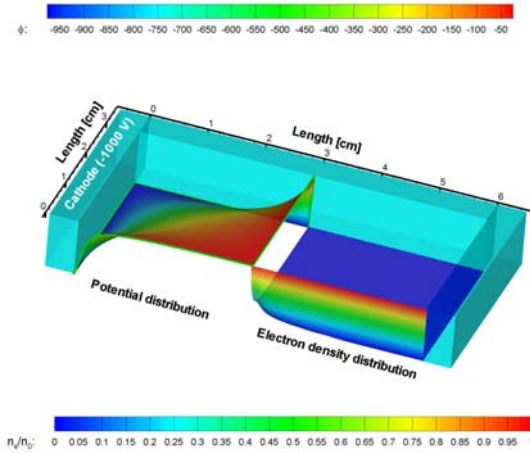


Fig. 7. The potential and electron number density distributions of the U-shaped electrode including a schematic of the electrodes. The bulk plasma density, n_0 is 10^{18}m^{-3} and the neutral background density, n_n is 10^{20}m^{-3} . The cathode is at -1,000 V potential.

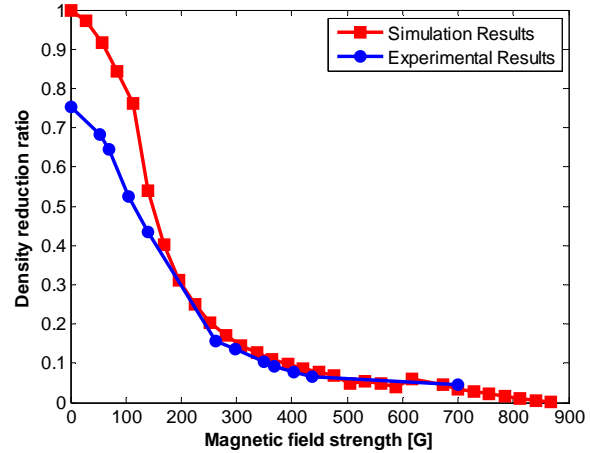


Figure 8. Model prediction vs. experimental data with varying magnetic field strength.

Figure 7 shows the calculated distribution of the electron density and potential near the two types of electrodes. The electron number densities are normalized by the bulk electron density n_0 . The electron density distribution shows the depleted region, the ‘hole.’ The ‘hole’ region indicates the area of almost zero electron density. It illustrates a possibility for solving the communication blackout problem with a two-dimensional shaped cathode (i.e., if the low-density region near the electrode becomes comparable to the antenna size, then radio wave communication should be possible through the plasma layer).

Comparison between the experimental results and the model predictions in the case of the electromagnetic mitigation approach is shown in Fig. 8. The density reduction of the experimental data is calculated by taking the ratio of the ion saturation currents with and without -100 V on the electrodes with the magnetic field on for both measurements.²¹ At the weak magnetic field condition, the model predicts a slightly higher density reduction ratio than the experimental results, while agreement is very good in the case of a high magnetic field. Based on these results it can be concluded that electromagnetic approach leads to plasma density reduction

which is significant for telemetry. One can conclude that both mitigation approaches, namely electrostatic and electromagnetic, can lead to electron density reduction thus increasing the frequency range that allows communication without significant attenuation.

CONCLUSIONS

This paper has described a model for nanosecond pulsed laser ablation of an aluminum target. This model describes the laser-solid interaction that results in target heating and vaporization leading to ablation. The results include the temperature distribution in the aluminum target, the surface temperature profile, the ablation rate and the amount of evaporation. Studies indicate that for fluences above this range, laser absorption by the plasma created by the ablation becomes significant and has to be taken into account. The electrostatic mitigation approach takes into account that an electron depleted sheath is formed around the negatively biased electrode. This creates a 'hole' in the electron density distribution allowing radio communication through the plasma. On the other hand electromagnetic mitigation approach is based on plasma acceleration in the ExB layer and consequent plasma density reduction. Both mitigation approaches can lead to electron density reduction thus increasing the frequency range that allows communication without significant attenuation.

REFERENCES

1. Radziemski, L. J. and D. A. Cremers, *Laser-Induced Plasmas and Applications*. Marcel Dekker, Inc. (1989)
2. Keidar, M., I. D. Boyd, and I. I. Beilis, *On the model of Teflon ablation in an ablation controlled discharge*, J. Phys. D: Appl. Phys. **34**, 1675 (2001)
3. von Allmen, M., *Laser Beam Interactions with Materials*. Springer Heidelberg (1987)
4. Semak, V.V. and T. F. Miller, *Modeling of laser charring and material removal in fiberglass materials*, J. Directed Energy **2**(1), 5 (2006)
5. Dushman, S., *Vacuum Techniques*. John Wiley & Sons, Inc. (1949)
6. Keidar, M., J. Fan, I. D. Boyd, and I. I. Beilis, *Vaporization of heated materials into discharge plasmas*, J Appl. Phys. **89**(6), 3095 (2001)
7. Anisimov, S.I. *Vaporization of metal absorbing laser radiation*, Sov. Phys. JETP **27**, 182 (1968)
8. Peterlongo, A., A. Miotello, and R. Kelly, *Laser-pulse sputtering of aluminum: vaporization, boiling, superheating and gas dynamics effects*, Phys. Rev. E **50**(6), 4716 (1994)
9. Amoroso, S., *Modeling of UV pulsed laser ablation of metallic surfaces*, Appl. Phys. A **69**, 323 (1999)
10. Mele, A., A. G. Guidoni, R. Kelly, C. Flamini, and S. Orlando, *Laser ablation of metals: analysis of surface heating and plume expansion experiments*, Appl. Surf. Sci. **109**, 584 (1997)

11. Yilbas, B. S., *Numerical approach to pulsed laser heating of semi-infinite aluminum substance*, Heat and Mass Trans. **31**, 279 (1996)
12. Bogaerts, A., Z. Chen, R. Gijbels, and A. Vertes, *Laser ablation for analytical sampling what can we learn from modeling ?* Spectrochimica Acta Part B **58**, 1867 (2003)
13. Keidar, M., I. D. Boyd, J. Luke, and C. Phipps, *Plasma generation and plume expansion for a transmission-mode micro-laser ablation plasma thruster*, J. Appl. Phys. **96**(1), 49 (2004)
14. Boardman, A. D., B. Cresswell, and J. Anderson, *An analytical model for the laser ablation of materials*, Appl. Surf. Sci. **96-98**, 55 (1996)
15. Leboeuf, J. N., K. R. Chen, J. M. Donato, D. B. Geohegan, C. L. Liu, A. A. Puretzky, and R. F. Wood, *Modeling of dynamical processes in laser ablation*, Appl. Surf. Sci. **96-98**, 14 (1996)
16. Ho, J. R., C. P. Grigoropoulos, and J. A. C. Humphrey, *Computational Study of Heat Transfer and Gas Dynamics in the Pulsed Evaporation of Metals*, J. Appl. Phys., 78 (7) 4696-4709 (1995)
17. Gusarov Andry V., Alexy G. Gnedovets and Igor Smurov, *Gas Dynamics of Laser Ablation: Influence of Ambient Atmosphere*, J. Appl. Phys., 88 (7) 4352-4364 (2000)
18. Gusarov Andry V., and Igor Smurov, *Thermal Model of Nanosecond Pulsed Laser Ablation: Analysis of Energy and Mass Transfer*, J. Appl. Phys., 97, 014307 (2005)
19. Rajendran S., M. Keidar, and I. D. Boyd, *Ablation and Plasma Formation Due to Laser Irradiance*, AIAA Plasmadynamic Conference, June 2007, Miami, Florida, Paper AIAA-2007-4378.
20. Tannehill, J. C., D. A. Anderson, and R. H. Pletcher, *Computational Fluid Mechanics and Heat Transfer*. Taylor & Francis (1997)
21. Kim, M., M. Keidar, I. D. Boyd, and D. Morris, *Plasma Density Reduction Using an Electromagnetic ExB Fields During the Reentry Flight*, Intern. Telemetry Conference, Las Vegas Nevada, October 2007.